Journal of Statistical Mechanics: Theory and Experiment
An IOP and SISSA journal

Multifractal analysis of sunspot time series: the effects of the 11-year cycle and Fourier truncation

Jing Hu[1,2], **Jianbo Gao**[1] **and Xingsong Wang**[3]

[1] Department of Electrical and Computer Engineering, University of Florida, Gainesville, FL 32611, USA
[2] Affymetrix, 3380 Central Expressway, Santa Clara, CA 95051, USA
[3] School of Mechanical Engineering, Southeast University, Nanjing 211189, People's Republic of China
E-mail: jinghu@ufl.edu, gao@ece.ufl.edu and xswang@seu.edu.cn

Received 6 August 2008
Accepted 27 January 2009
Published 27 February 2009

Online at stacks.iop.org/JSTAT/2009/P02066
doi:10.1088/1742-5468/2009/02/P02066

Abstract. Multifractal theory provides an elegant statistical characterization of many complex dynamical variations in Nature and engineering. It is conceivable that it may enrich characterization of the sun's magnetic activity and its dynamical modeling. Recently, on applying Fourier truncation to remove the 11-year cycle and carrying out multifractal detrended fluctuation analysis of the filtered sunspot time series, Movahed *et al* reported that sunspot data are characterized by multifractal scaling laws with the exponent for the second-order moment, $h(2)$, being 1.12. Moreover, they think the filtered sunspot data are like a fractional Brownian motion process with anti-persistent long-range correlations characterized by the Hurst parameter $H = h(2) - 1 = 0.12$. By designing an adaptive detrending algorithm and critically assessing the effectiveness of Fourier truncation in eliminating the 11-year cycle, we show that the values of the fractal scaling exponents obtained by Movahed *et al* are artifacts of the filtering algorithm that they used. Instead, sunspot data with the 11-year cycle properly filtered are characterized by a different type of multifractal with persistent long-range correlations characterized by $H \approx 0.74$.

Keywords: new applications of statistical mechanics

Contents

1. Introduction

A sunspot, sometimes as large as 50 000 miles in diameter, is a dark part of the sun's surface that is cooler than the surrounding area [1]. It is cooler because the magnetic field there is so strong that it inhibits the transport of heat via convective motion in the sun. The magnetic field is formed below the sun's surface and extends out into the sun's corona. Its strength at a typical point on the solar surface is a few gauss. However, it can be much higher in sunspots. In fact, sometimes the magnetic field there is so strong that solar flares occur. Solar flares cause geomagnetic storms, which affect the earth in numerous significant ways.

One fascinating property of sunspots is the approximate 11-year cycle, which can be easily seen from the monthly sunspot data that can be downloaded from SIDC's website (http://sidc.oma.be/sunspot-data/). This is shown as black curves in figures 1(a)–(c). Because of this cycle, a beautiful pattern, called a Maunder 'butterfly' diagram, emerges in the time–latitude distribution when sunspots move across the surface of the sun, expanding, contracting, and approaching the equator [2, 3].

To this day, sunspots remain the best known manifestation of solar magnetic activity and its cycle, and thus have been a subject of extensive research. Indeed, sunspots and related activities have been analyzed by various methods, including correlation analysis [4, 5], chaos analysis [6, 7], and multifractal analysis [8]–[10]. Multifractal theory provides an elegant statistical characterization of many complex dynamical variations in Nature and engineering [11, 12]. It is conceivable that it may enrich characterization of the sun's magnetic activity and its dynamical modeling (e.g., the sun's dynamo model [13]). Recently, a particularly noteworthy work has been reported by Movahed *et al* [9]. From applying Fourier truncation to remove the low-frequency 11-year cycle and then carrying

doi:10.1088/1742-5468/2009/02/P02066

J. Stat. Mech. (2009) P02066

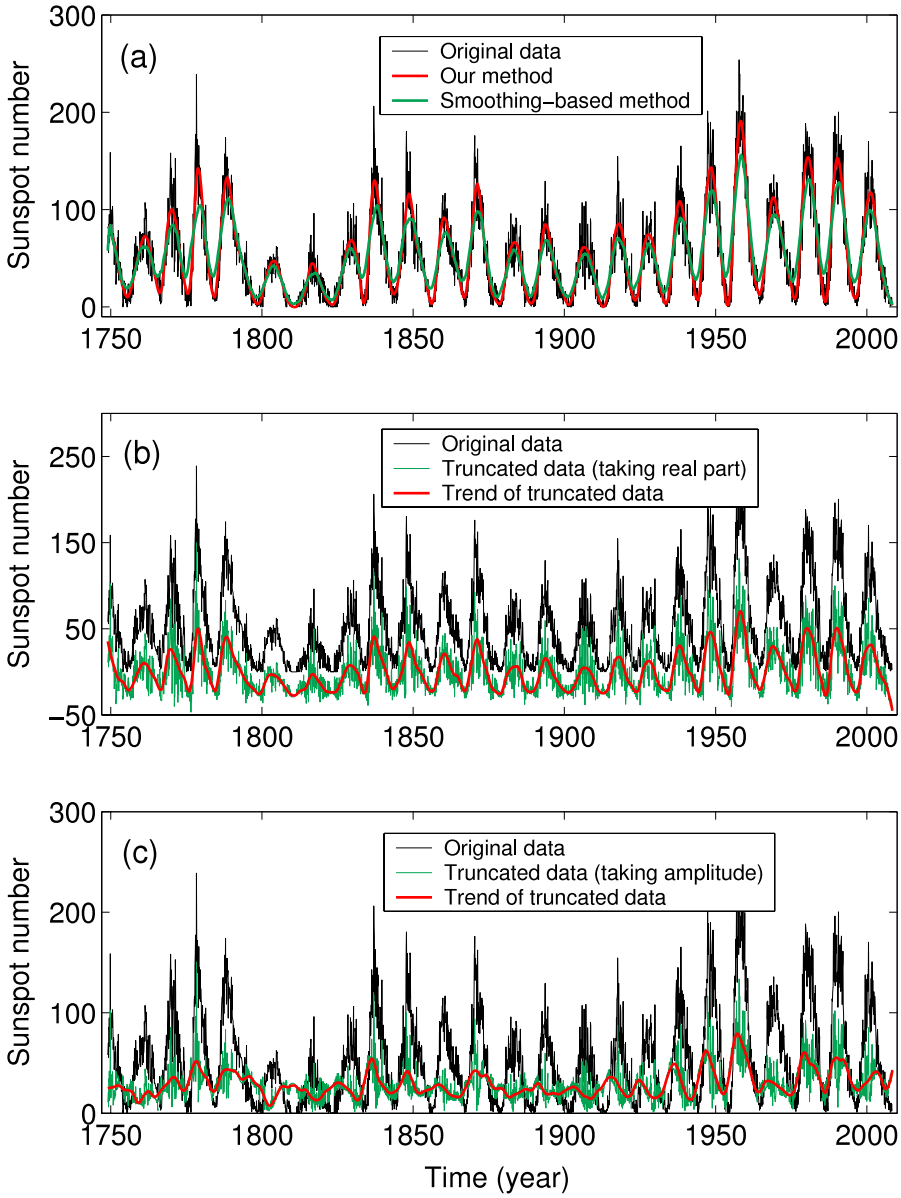

Figure 1. (a) Black curve: the original monthly sunspot data. Red and blue curves: trends obtained by adaptive detrending and smoothing, respectively. The window size for both cases is 61 months. (b) The black curve is the re-plot of the original sunspot data, the green one is the real part of the Fourier truncation filtered sunspot data, and the red one is the trend estimated from the green curve using the adaptive detrending algorithm. (c) Same as (b) except that the green curve is the amplitude of the Fourier truncation filtered sunspot data.

out multifractal detrended fluctuation analysis (MF-DFA) of the filtered sunspot time series, they conclude [9] that sunspot data are characterized by multifractal scaling laws with the exponent for the second-order moment, $h(2)$, being 1.12. Moreover, they think the filtered sunspot data are like a fractional Brownian motion (fBm) process, and therefore, the increment process obtained by differencing the filtered sunspot data

(which they call the fluctuations of the sunspot variations) has anti-persistent long-range correlations with the Hurst parameter $H = h(2) - 1 = 0.12$. As we shall show in the next section, the Fourier truncation employed in [9] was carried out at a timescale of five years. If Fourier truncation acts as an ideal high-pass filter, as Movahed *et al* wished, then it should have removed all information from the data on timescales beyond five years. As a consequence, the filtered sunspot data should not have fractal scalings on timescales longer than five years. Puzzlingly, the multifractal scaling behaviors reported in [9] are valid for timescales up to more than 50 years. This inconsistency compels us to question the relevance of the reported multifractality to sunspots: is it a genuine property of the sunspots or is it an irrelevant feature simply introduced by the specific filtering technique employed in [9]? By designing an adaptive detrending algorithm and critically assessing the effectiveness of Fourier truncation in eliminating trends, we shall show that the values of the fractal scaling exponents reported in [9] are indeed artifacts of the algorithm used there. Correctly detrended sunspot data are instead characterized by persistent long-range correlations with the Hurst parameter close to 0.74.

The remainder of the paper is organized as follows. In section 2, we discuss adaptive detrending and Fourier truncation for removing the 11-year cycle in sunspots. In section 3, first we review the basics of random fractal theory to a depth adequate for us to appreciate the significance and problems of [9], then we systematically carry out detrended fluctuation analysis (DFA) of the original sunspot data, as well as the trend and detrended data of sunspots; finally we carry out multifractal analysis of detrended sunspot data. Concluding discussions are contained in section 4.

2. Removing the 11-year cycle from sunspots through adaptive detrending and Fourier truncation

To facilitate assessment of the effectiveness of Fourier truncation in eliminating the 11-year cycle from sunspot data, we discuss our new adaptive detrending algorithm first.

2.1. Eliminating the 11-year cycle through adaptive detrending

Roughly, existing methods for finding trends may be classified into two groups, global and local. The majority of the global methods assume certain functional forms, such as linear, exponential, or polynomial functions for a trend, and hence, are extrinsic. An exception is the empirical mode decomposition (EMD) based method recently proposed by Wu *et al* [14], which estimates a trend by finding recursively, intrinsic features of the data (e.g., local extrema and zero-crossings), until a preset stoppage criterion is satisfied. Unfortunately, the EMD based method cannot be readily used to remove the 11-year cycle from sunspot data, since it is based on an assumption that a trend is a monotonic function having at most one extremum within a given data span, which is clearly not true with sunspot data.

Local detrending may be further classified into smoothing based and segmentation based. The former estimates a trend by taking the (weighted) moving average of the data. The latter segments the data and fits a local trend to each segment. The smoothing based method, although popular, is not very accurate, as is evident from the green curve in figure 1(a): comparing with the cycle perceived visually, the green curve does not track

J. Stat. Mech. (2009) P02066

the cycle effectively. Similarly, existing segmentation based local detrending methods are not good either, because they have jumps, discontinuities, or a lack of smoothness around the boundaries of neighboring segments.

The above discussions suggest that in order to develop an effective segmentation based local detrending algorithm, special care has to be taken around the boundaries of the neighboring segments to ensure that there are no discontinuities. We have devised a new local adaptive detrending algorithm with these properties. It first partitions a time series into segments (or windows) of length $2n+1$ points, where neighboring segments overlap by $n+1$ points. For each segment, we fit a best polynomial of order K. Note that $K=0$ and 1 correspond to piecewise constant and linear fitting, respectively. Denote the fitted polynomials for the ith and $(i+1)$th segments by $y^{(i)}(l_1)$, $y^{(i+1)}(l_2)$, $l_1, l_2 = 1, \ldots, 2n+1$, respectively. Note that the length of the last segment may be smaller than $2n+1$. We define the trend for the overlapped region as

$$y^{(c)}(l) = \left(1 - \frac{l-1}{n}\right) y^{(i)}(l+n) + \frac{l-1}{n} y^{(i+1)}(l), \qquad l = 1, 2, \ldots, n+1. \tag{1}$$

The weights, which decrease linearly with the distance between the point and the center of the segment, effectively eliminate any jumps or discontinuities around the boundaries of neighboring segments. In fact, the scheme ensures that the trend is smooth at the non-boundary points, and has at least the right- or left-derivative at the boundary points. Because of these properties, the window size, $2n+1$, does not impose an arbitrarily chosen external timescale.

Note that the method contains two free parameters, K, the order of the polynomial, and $2n+1$, the segment length (or window size)—by properly choosing K and making $2n+1$ small enough, the detrending can become a true fitting operation, since the detrended data can be precisely zero. When analyzing experimental data, both parameters may be determined by requiring that the variance of the detrended data no longer decreases significantly when K is further increased and/or $2n+1$ is further decreased. To illustrate the idea, in figure 2 we have shown the variation of the variance of the detrended data (normalized by that of the original sunspot data) with K, when the window size is set to 61, which is comparable to that used in [9]. We observe that $K=2$ already yields almost saturated small variance for the detrended data. The resulting trend is shown as the red curve in figure 1(a). Clearly, it identifies the 11-year cycle much more accurately than the smoothing based method (the green curve in figure 1(a)).

2.2. Eliminating the 11-year cycle through Fourier truncation

Fourier truncation for trend removal works as follows [9, 15]. First, the time series is transformed to the frequency domain. Then, the first few coefficients of the Fourier expansion are truncated (i.e., set to zero). Finally, the truncated Fourier series is inversely transformed to give a new time series. Assume that there are N points in a time series with a sampling time interval of δt. Then the frequency resolution is $1/(N\delta t)$. The Lth point in the frequency domain corresponds to a timescale of $(N/L)\delta t$. In [9], monthly sunspot data from 1749 to 2005 were analyzed. A truncation involving the first $L=50$ coefficients in the Fourier domain therefore involves a timescale of $N/L = 256 \times 12/50 \approx 60$ months.

The monthly sunspot data analyzed by us, from 1749 up to the present, are about 30 points longer than those analyzed in [9]. As expected, when processed by the Fourier

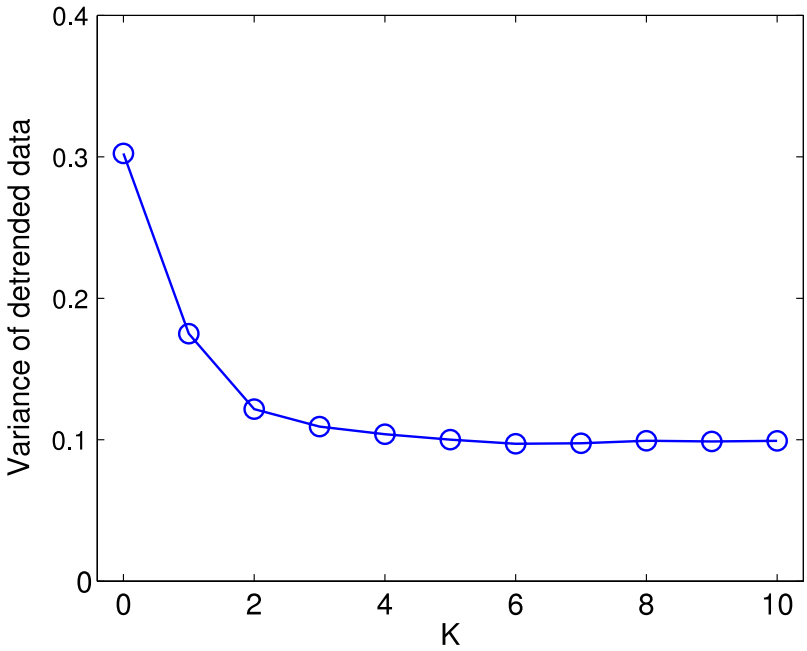

Figure 2. Variation of the variance of the detrended data of monthly sunspot data with the polynomial order K.

truncation method, the resulting time series is complex valued. The real part and amplitude of the complex time series are shown as the green curves in figures 1(b) and (c), respectively. We observe that neither the real part nor the amplitude eliminates the 11-year cycle completely. Instead, they only suppress the cycle to some degree. In fact, the remaining cyclic trends can be readily obtained by using our adaptive detrending algorithm; they are shown as the red curves in figures 1(b) and (c), respectively.

Why can Fourier truncation not effectively eliminate the 11-year cycle from sunspot data? The reason is that ideal high-pass (and low-pass) filters, which are equivalent to simply setting the low-frequency (and high-frequency) coefficients to zero, are not physically realizable (which is equivalent to Heisenberg's uncertainty principle). One manifestation is that the inversely transformed time series is usually complex valued, as we have seen here. Therefore, multifractality of sunspot data filtered through Fourier truncation may not represent properties of sunspots at all. This point will be made much clearer in section 3.

3. Multifractal detrended fluctuation analysis of sunspot data

In this section, first we review the basics of random fractal theory in depth so that we can fully appreciate the significance and problems of [9], then we systematically carry out DFA of the original sunspot data, as well as the trend and detrended data of sunspots; finally we carry out multifractal DFA of detrended sunspot data.

3.1. Basics of random fractal theory

Of the types of activity that characterize complex systems, the most ubiquitous and puzzling is perhaps the appearance of $1/f^{\alpha}$ noise, a form of temporal or spatial fluctuation

characterized by a power-law decaying power spectral density [12]. Let $X = \{X_t\colon t = 0, 1, 2, \ldots\}$ be a covariance stationary stochastic process with mean μ, variance σ^2, and autocorrelation function $r(k), k \geq 0$. The process is said to have long-range correlation [12] if $r(k)$ is of the form

$$r(k) \sim k^{2H-2}, \qquad \text{as } k \to \infty, \tag{2}$$

where $0 < H < 1$ is the Hurst parameter. Note that when $1/2 < H < 1$, $\sum_k r(k) = \infty$. This justifies the term 'long-range correlation'.

Next we construct a new covariance stationary time series $X^{(m)} = \{X_t^{(m)}\colon t = 1, 2, 3, \ldots\}$, $m = 1, 2, 3, \ldots$, obtained by averaging the original series X over non-overlapping blocks of size m,

$$X_t^{(m)} = (X_{tm-m+1} + \cdots + X_{tm})/m, \qquad t \geq 1. \tag{3}$$

Note that the length of $\{X_t^{(m)}\}$ is $[N/m]$, where N is the length of $\{X_t\}$, and $[\,]$ denotes the greatest integer function. Denote the variance of $X_t^{(m)}$ by $V_m = \mathrm{var}(X^{(m)})$. It can be proven that

$$\mathrm{var}(X^{(m)}) = \sigma^2 m^{2H-2}. \tag{4}$$

Equation (4) is often called the variance–time relation. To understand its significance, let us explain the 'little smoothing' behavior: when $H = 0.5$, $\mathrm{var}(X^{(m)})$ drops to $10^{-2}\sigma^2$ when $m = 100$, where σ^2 is the variance of the original process; when $H = 0.75$, in order for $\mathrm{var}(X^{(m)})$ to drop as much, m has to be 10 000. On the other hand, when $H = 0.25$, $\mathrm{var}(X^{(m)})$ drops to $10^{-2}\sigma^2$ when $m \approx 23$. Therefore, when H increases, smoothing becomes less effective in reducing the variance of the process.

Note that the power spectral density (PSD) for X is

$$S_X(f) \sim f^{-(2H-1)}. \tag{5}$$

Therefore, X is called a $1/f^\alpha$ process. Its integration, called the random walk process (see below), has PSD $f^{-(2H+1)}$.

The prototypical random walk model for $1/f^\alpha$ process is the fBm process, $B_H(t)$, where H is the Hurst parameter [16]. It is a Gaussian process with mean 0, stationary increments, variance

$$E[(B_H(t))^2] = t^{2H} \tag{6}$$

and covariance

$$E[B_H(s)B_H(t)] = \tfrac{1}{2}\{s^{2H} + t^{2H} - |s-t|^{2H}\}. \tag{7}$$

The increment process of the fBm, $X_i = B_H((i+1)\Delta t) - B_H(i\Delta t)$, $i \geq 1$, where Δt can be considered a sampling time, is called fractional Gaussian noise (fGn). It is a zero-mean stationary Gaussian time series, with autocorrelation function

$$\gamma(k) = E(X_i X_{i+k})/E(X_i^2) = \tfrac{1}{2}\Big\{(k+1)^{2H} - 2k^{2H} + |k-1|^{2H}\Big\}, \qquad k \geq 0. \tag{8}$$

Since $\gamma(k)$ is independent of Δt, without loss of generality, we can take $\Delta t = 1$. In particular, we have $\gamma(1) = \frac{1}{2}(2^{2H} - 2)$. The notions of persistent and anti-persistent

correlations come from the fact that $\gamma(1)$ is positive when $1/2 < H < 1$, but negative when $0 < H < 1/2$. When $k \to \infty$, $\gamma(k) \sim k^{2H-2}$.

We now consider estimation of H. A convenient framework is based on the random walk process y, defined as

$$y_k = \sum_{i=1}^{k} (X_i - \bar{X}), \tag{9}$$

where $\bar{X}$ is the mean of X. We then examine whether the following scaling laws hold or not:

$$F^{(q)}(m) = \langle |y(i+m) - y(i)|^q \rangle^{1/q} \sim m^{H(q)}, \tag{10}$$

where q is real and the average is taken over all possible pairs of $(y(i+m), y(i))$. Note that $q > 0$ emphasizes large absolute value, while $q < 0$ emphasizes small absolute value (to better understand this statement, it is helpful to think about concrete cases such as $q = 10$ and -10). When $H(q)$ is a constant, the process is called a monofractal; otherwise, it is called a multifractal. The case of $q = 2$ is of special interest, since $H(2) = H$. In this case, equation (10) is often called fluctuation analysis (FA). It is equivalent to many other methods, including analysis based on the variance–time relation, R/S statistic, Fano factor analysis, and a few others [11, 12]. The largest scaling exponent that can be estimated using these methods is 1 [11, 12]. Many processes, including auto-regressive processes, ON/OFF models, Levy walks, and processes with trends, contain certain timescale range where the scaling exponent can be larger than 1. To accurately estimate those exponents, DFA and wavelet multi-resolution analysis are recommended [11, 12, 17]. For simplicity, we only describe DFA and its multifractal version here. Details on wavelet multi-resolution analysis can be found in [12, 17].

DFA works as follows [18]: (i) construct a random walk process from the original data using equation (9); (ii) divide a given random walk of length N into $[N/m]$ non-overlapping segments (where the notation $[\ ]$ denotes the largest integer that is not greater than x); (iii) define the local trend in each segment to be the ordinate of a linear least-squares fit for the random walk in that segment; (iv) compute the 'detrended walk', denoted by $y_m(n)$, as the difference between the original walk $y(n)$ and the local trend. Then one examines

$$F_d(m) = \left\langle \sum_{i=1}^{m} y_m(i)^2 \right\rangle^{1/2} \sim m^H, \tag{11}$$

where the angle brackets denote average of the $[N/m]$ segments. Therefore, $F_d(m)$ is the square root of the average variance over all segments.

Before proceeding, we make three comments. (1) The above description of DFA involves non-overlapping segmentation of a data set. There are two kinds of edge effects. One corresponds to the case where N/m is not an integer, i.e., $N = pm + r$, where $p > 0$, $0 < r < m$. This effect, which typically is not serious, can be remedied by applying DFA to the data set twice, once from the first point to the pmth point, the other time from the $(r+1)$th point to the Nth point, and taking the average. The other edge effect is because of the non-overlapping segmentation. This effect can be remedied by using overlapping segmentation instead of non-overlapping segmentation. However,

overlapping segmentation slows down computation greatly, and therefore, is seldom used. In the following, we shall use DFA in its original, simple form. Its effectiveness can be appreciated by examining a few fractal processes with known properties, as we shall show shortly. (2) When DFA is applied to a fGn-like process, one obtains the correct H. If the original data, denoted by the X process, are already like a fBm-type random walk process, then the first step of DFA amounts to an additional integration, and DFA yields a scaling exponent of $H+1$ [11, 12] (see also the appendix of [9]). (3) A sinusoidal trend, which is most relevant to the 11-year cycle in sunspots, corresponds to a scaling exponent of 2 [19]. As we have mentioned, the largest H from FA (and its equivalent versions) is 1. In this regard, DFA is a more robust method.

We now explain how to extend DFA to MF-DFA. Depending on how the deviation from a straight line in each window is quantified, one can have (at least) two forms. One is given by

$$F_d^{(q)}(m) = \left\langle \sum_{i=1}^{m} |y_m(i)|^q \right\rangle^{1/q} \sim m^{H(q)}, \tag{12}$$

where q is real, taking on both negative and positive values. Another is given by

$$F_d^{(q)}(m) = \left\langle \left[\sum_{i=1}^{m} |y_m(i)|^2 \right]^{q/2} \right\rangle^{1/q} \sim m^{H(q)}. \tag{13}$$

The first formulation amounts to using the l_1 norm, while the second uses the l_2 or the Euclidean norm. When $H(q)$ is constant in q, we say the data constitute a monofractal. Otherwise, they constitute a multifractal.

To check how well multifractal DFA characterizes monofractal processes with known $H(q)$ spectrum, let us use the formulation based on equation (12) to examine fBm processes with $H = 0.25$ and 0.75, as well as the integration of these fBm processes. The results are shown in figures 3 and 4, respectively. We observe that the method correctly estimates H (including the case of $H > 1$) as well as demonstrating the monofractal nature of fBm processes and their integrations. We also note that when $q < 0$, the scaling becomes not good. This is a common feature shared by wavelet multifractal analysis, however (see [17], especially figures 3, 6, 10 there).

The above multifractal formulation is based on the structure–function technique. Another framework is based on the thermodynamic formulation. The basic idea is to consider the scaling exponents for the qth moments of the measure μ [12, 17]:

$$Z(q,\epsilon) = \sum_{i=1}^{N(\epsilon)} \mu_i^q(\epsilon) \sim \epsilon^{\tau(q)}, \qquad \epsilon \to 0, \tag{14}$$

where $N(\epsilon)$ is the number of boxes of size ϵ needed to cover the support of the measure μ. The spectrum of generalized dimensions D_q is defined by

$$D_q = \frac{\tau(q)}{q-1}, \tag{15}$$

where D_0 is the capacity (or box-counting) dimension, and D_1 is the information dimension. When $D(q)$ is constant in q, the measure is called monofractal; otherwise, it is called multifractal.

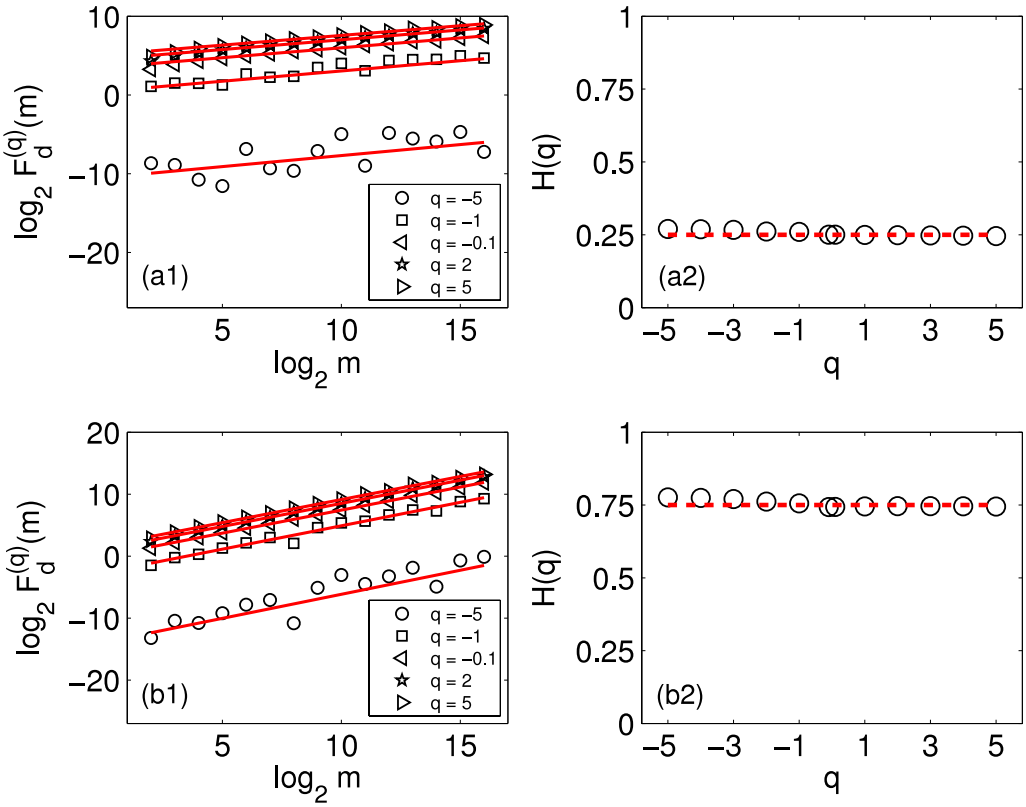

Figure 3. Multifractal DFA of fBm processes with $H = 0.25$ ((a1), (a2)) and $H = 0.75$ ((b1), (b2)).

Alternatively, one may characterize the measure via the singular spectrum $f(\alpha)$, which is the dimension of points with pointwise dimension α. It is related to $\tau(q)$ via a Legendre transform,

$$q = \mathrm{d}f(\alpha)/\mathrm{d}\alpha, \qquad \tau(q) = q\alpha - f(\alpha). \tag{16}$$

Combining equations (15) and (16), we have

$$D_q = \frac{1}{q-1}[q\alpha(q) - f(\alpha(q))]. \tag{17}$$

Therefore, D_q and $f(\alpha)$ give the same amount of information.

To better understand the measure based multifractal formulation, it is instructive to consider the random cascade model. This type of multifractal was initially developed to understand the intermittent features of turbulence [20]–[22]. Mandelbrot was among the first to introduce this concept [23]. Parisi and Frisch's work [24] has made it widely known. For simplicity, we shall follow the presentations of our earlier work on traffic modeling [12, 25, 26] and geophysical data modeling [27].

Consider a unit interval. Associate it with a unit mass. Divide the unit interval into two, say, left and right segments of equal length. Also, partition the associated mass into two fractions, r and $1-r$, and assign them to the left and right segments, respectively. The parameter r is in general a random variable, governed by a probability density function

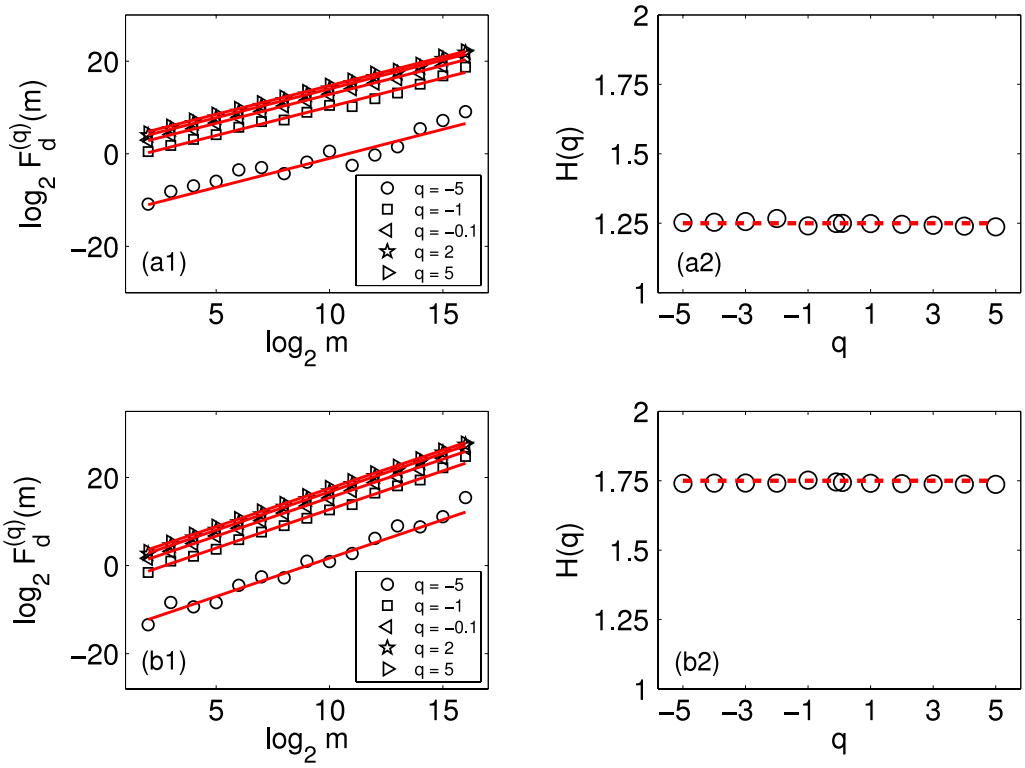

Figure 4. Multifractal DFA of integration of fBm processes with $H = 0.25$ ((a1), (a2)) and $H = 0.75$ ((b1), (b2)).

(PDF) $P(r)$, $0 \leq r \leq 1$. The fraction r is called the multiplier. Each new subinterval and its associated weight are further divided into two parts following the same rule. This procedure is schematically shown in figure 5, where the multiplier r is written as r_{ij}, with i indicating the stage number and j (assuming only odd numbers, leaving even numbers for $1-r_{ij}$) indicating the positions of a weight on that stage. Note that the scale (i.e., the interval length) associated with stage i is 2^{-i}. We assume that $P(r)$ is symmetric about $r = 1/2$ and has successive moments $\mu_1, \mu_2, \ldots$. Hence r_{ij} and $1 - r_{ij}$ both have marginal distribution $P(r)$. The weights at the stage S, $\{w_n, n = 1, \ldots, 2^S\}$, can be expressed as

$$w_n = u_1 u_2 \cdots u_S,$$

where u_l, $l = 1, \ldots, S$, are either r_{ij} or $1 - r_{ij}$. Thus, $\{u_i, i \geq 1\}$ are independent, identically distributed random variables having PDF $P(r)$. In particular, at stage S, we have

$$M_q(\epsilon) = \sum_{n=1}^{2^S} (w_n)^q \approx 2^S E(w^q) = 2^S E((u_1 u_2 \cdots u_S)^q) = 2^S \mu_q^S \sim \epsilon^{\tau(q)}, \tag{18}$$

where E denotes expectation. Using $\epsilon = 2^{-S}$, we then obtain

$$\tau(q) = -\ln(2\mu_q)/\ln 2. \tag{19}$$

We may treat the weights at a sufficiently large stage number (say, S) as a fGn-like process, and analyze it using the structure–function based multifractal formulation. For

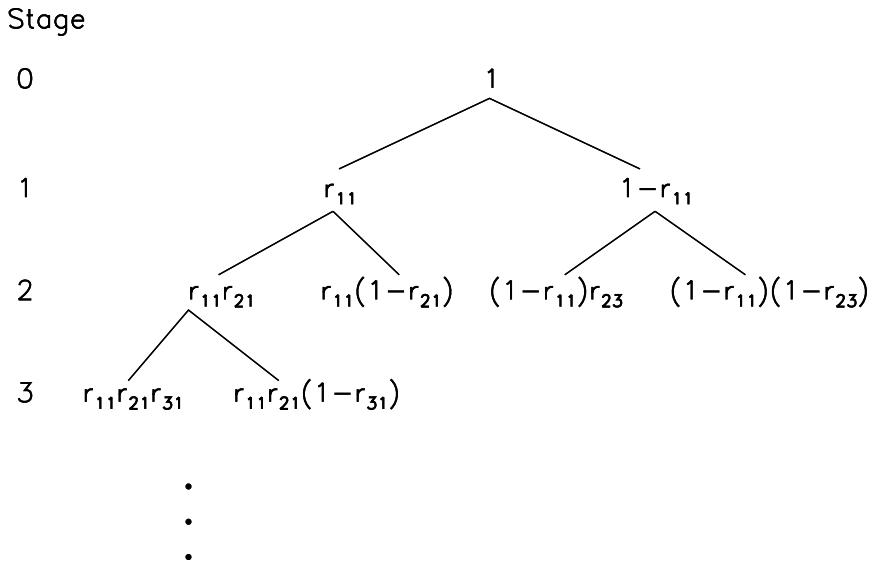

Figure 5. Schematic illustrating the construction rule of a multiplicative multifractal.

simplicity, let us focus on the case of $m = 2^k$ when using equation (10), where k is an integer. Here, $y(i+m) - y(i)$ amounts to a weight at stage $S - k$. Therefore,

$$F^{(q)}(m) = (\mu_q^{S-k})^{1/q} \sim m^{H(q)}. \tag{20}$$

To a good approximation, we may drop the term involving S. Then, using $m = 2^k$, we have

$$H(q) \sim -\frac{1}{q} \ln \mu_q / \ln 2 \tag{21}$$

and

$$\tau(q) = qH(q) - 1. \tag{22}$$

Therefore, $\tau(q)$ and $H(q)$ give the same amount of information about cascade processes.

We now illustrate equations (19) and (21) with a concrete example. For this purpose, let us consider the random binomial model, which is specified by a multiplier distribution $P(r)$ to be

$$P(r) = [\delta(r-p) + \delta(r-(1-p))]/2 \tag{23}$$

so that $P(r = p) = P(r = 1-p) = 1/2$. Here, the qth moment $\mu_q = [p^q + (1-p)^q]/2$. Therefore,

$$\tau(q) = -\ln[p^q + (1-p)^q] / \ln 2 \tag{24}$$

and

$$H(q) = \frac{1}{q}\{1 - \ln[p^q + (1-p)^q] / \ln 2\}. \tag{25}$$

Without loss of generality, we assume $p \leq 1/2$; then H attains maximal and minimal values of $-\ln p / \ln 2 > 1$ and $-\ln(1-p)/\ln 2 < 1$, when $q \to -\infty$ and ∞, respectively.

doi:10.1088/1742-5468/2009/02/P02066

J. Stat. Mech. (2009) P02066

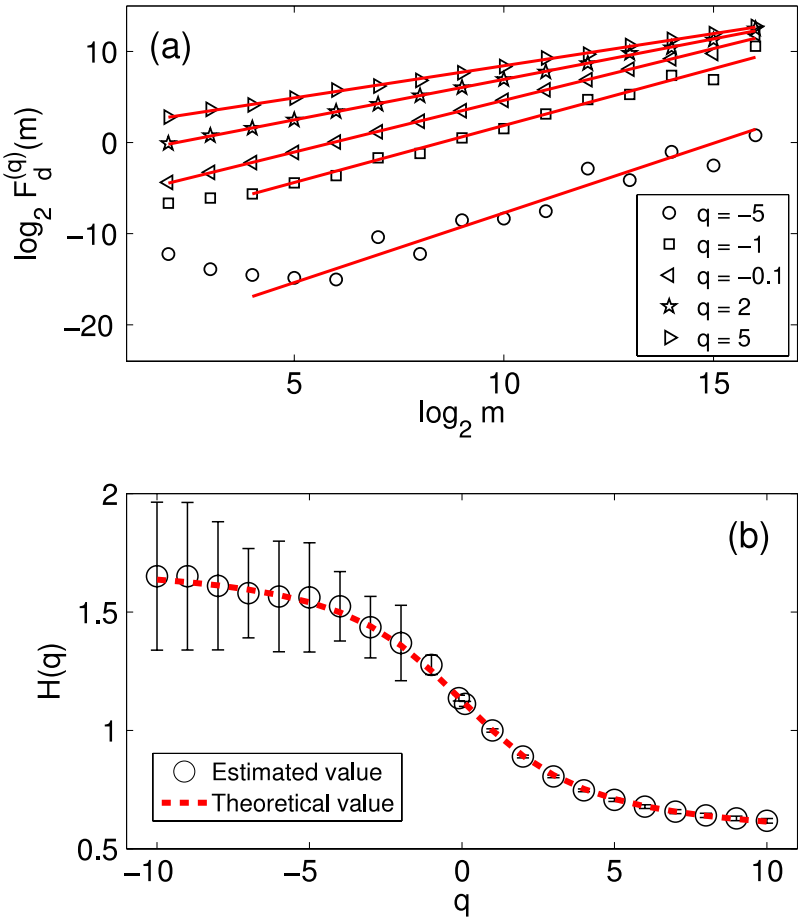

Figure 6. (a) Multifractal DFA of the binomial multifractal; (b) $H(q)$ spectrum from simulation (open circles) and theory (dashed line).

The derivation of equation (20) is based on equation (10), not based on multifractal DFA. Therefore, it is important to examine whether multifractal DFA can bring out the same result. We thus have analyzed the binomial multifractal using equation (12). Figure 6 shows the results of a binomial multifractal process with $p = 0.3$. We observe that the $H(q)$ spectrum estimated from simulations matches very well with equation (25), except that the scaling for $q < 0$ is not good, as can be seen from the bottom-most curve in figure 6(a) and the large error bars in figure 6(b) for $q < 0$. As we have pointed out earlier, the bad scaling for $q < 0$ is a common feature shared by wavelet based multifractal analyses [17]. Note that this is not a serious problem, as long as one is mainly concerned about large variations in sunspots.

3.2. DFA of fractal signals with trends

To perform fractal analysis of sunspot-like data with trends, it is important to first understand the behavior of DFA of fractal processes with trends. For this purpose, we have constructed 'compound' processes by superimposing trends on fGn processes and binomial multifractal processes. We have found that when the trend is simple, such as

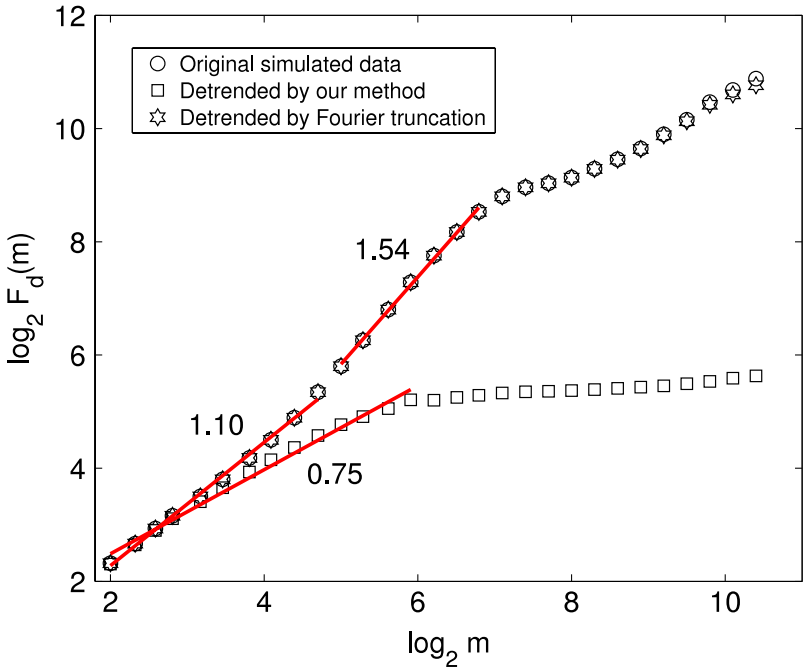

Figure 7. DFA of a 'compound' process obtained by superimposing the adaptively obtained trend of the sunspot data to a fGn process of $H = 0.75$ (circles), and DFA of the compound process filtered by Fourier truncation (pentagons) and by the adaptive detrending (squares).

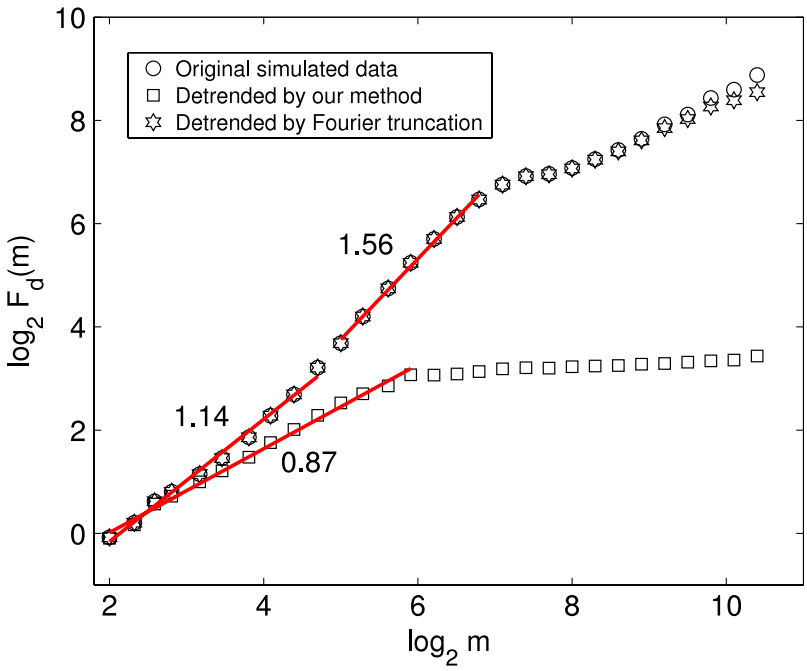

Figure 8. Same as figure 7 except now the original fractal process is a binomial multifractal process analyzed in figure 6 rather than a fGn process of $H = 0.75$.

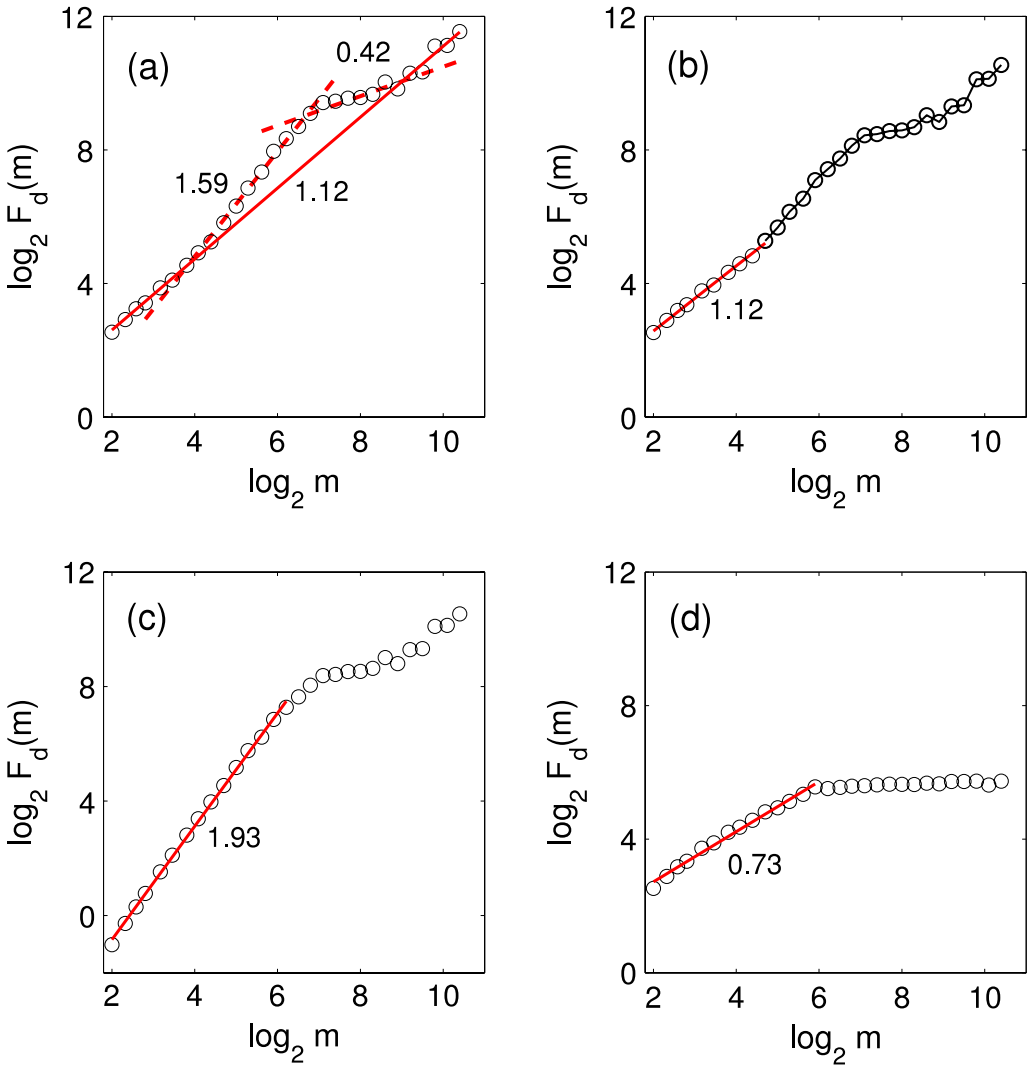

Figure 9. $\log_2 F_d(m)$ versus $\log_2 m$ curves for (a) the original sunspot data, (b) the Fourier truncation filtered sunspot data, (c) the trend of the Fourier truncation filtered sunspot data, and (d) the detrended form of the Fourier truncation filtered sunspot data. The H parameter is indicated as the slope of the least linear squares fit to the linear segments of the curves.

an ideal sinusoidal signal, Fourier truncation and adaptive detrending perform similarly well. However, when the trend becomes complicated, in the sense that it contains a lot of harmonics, the two methods behave markedly differently. To illustrate the idea, we have superimposed the adaptively obtained trend of sunspot data on fGn and binomial multifractal processes in such a way that the variances of the fractal processes are equal to 1/4 of the variance of the trend (observing figure 2, this means that the trend here is actually not as strong as that in the original sunspot data). The results are shown in figures 7 and 8. We observe that the results of DFA of the compound processes and the processes filtered by the Fourier truncation are essentially the same. Therefore, Fourier truncation fails in this situation. On the other hand, adaptive detrending correctly removes the superimposed trend and gets the correct H parameter.

doi:10.1088/1742-5468/2009/02/P02066

J. Stat. Mech. (2009) P02066

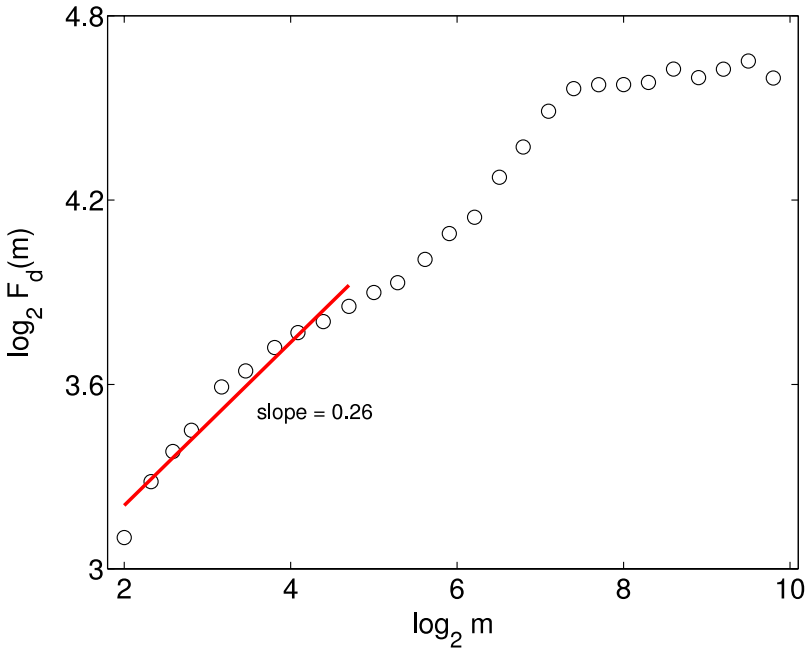

Figure 10. $\log_2 F_d(m)$ versus $\log_2 m$ curve for the increment process of the Fourier truncation filtered sunspot data.

Finally, we note that when the adaptive sunspot trend becomes weaker or stronger in the compound process, while adaptive detrending always performs as desired, Fourier truncation gives smaller or larger H values that are essentially the same as that of the compound process. The variation of the H for the compound process with the strength of the trend can be understood by the fact that the trend gives $H = 2$—when the trend becomes stronger, the weight for $H = 2$ becomes larger.

3.3. DFA of sunspot data filtered by Fourier truncation

Since the monthly sunspot data analyzed here are slightly longer than those analyzed in [9], it is worth comparing the DFA of the data analyzed here with that of [9]. Figure 9(a) shows $\log_2 F_d(m)$ versus $\log_2 m$ for the original sunspot data. We clearly observe three scaling regimes, the same as those reported in [9]. When the sunspot data are filtered by Fourier truncation with the first 50 coefficients set to zero, irrespective of whether we use the real part or the amplitude of the filtered data, we always observe a nice scaling behavior. Since the scaling behavior for the real part of the filtered data is the same as the amplitude of the filtered data, for ease of illustration, we shall only present the results based on the real part of the filtered data. Figure 9(b) shows the result for the filtered data, which is again the same as that reported in [9] (as well as being comparable to the slopes shown in figures 7 and 8 (pentagons)). What is more interesting is the DFA result of the trend data (i.e., the red curve in figure 1(b)) as well as the detrended data of the Fourier truncation filtered sunspot data (equivalent to the difference between the green and red curves of figure 1(b)). The results are shown in figures 9(c) and (d), respectively. We observe that for the trend data, the scaling exponent is 1.93, close to that

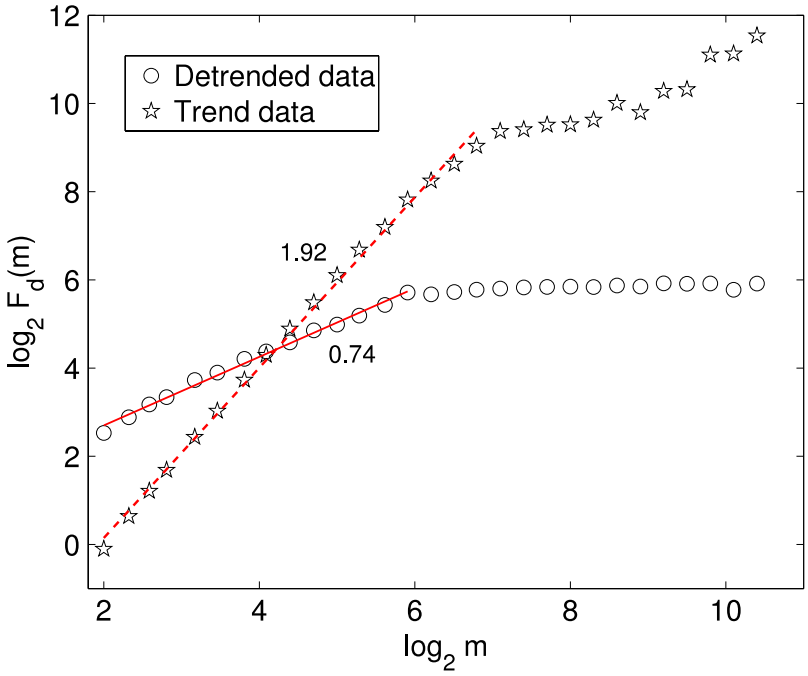

Figure 11. $\log_2 F_d(m)$ versus $\log_2 m$ curves for the adaptive trend and the adaptively filtered sunspot data.

of a sinusoidal trend, which is 2, as we mentioned earlier [19]. The scaling exponent for the detrended data, however, is only 0.73, much smaller than the 1.12 shown in figure 9(b).

Two important features in figure 9 are worth emphasizing. (i) The slope of 1.12 shown in figure 9(b) can be viewed as a certain weighted average of the slopes shown in figures 9(c) and (d) (in fact, the average is also scale dependent: the slope of figure 9(c) weighs more when $m > 2^6$ than when $m < 2^6$). (ii) The scaling of figure 9(d) is only valid for m slightly smaller than $2^6 = 64$ months. This is consistent with the fact that a timescale of 60 months is used in carrying out Fourier truncation. Therefore, $H = 0.73$ is indicative of the true fractal scaling exponent of properly detrended sunspot data. We shall come back to this point in section 3.4.

Movahed *et al* [9] argue that the Fourier truncation filtered sunspot data are like a fBm-type random walk process characterized by a scaling exponent of 1.12. If their conjecture is correct, then the increment process of the Fourier truncation filtered sunspot data, which is obtained by differencing the Fourier truncation filtered sunspot data, should be like a fGn noise. In other words, if one applies DFA to the increment process, or equivalently, if one applies DFA to the Fourier truncation filtered data without further integration (i.e., omitting the first step in DFA description), then one should observe a scaling exponent of $H = 0.12$ [11, 12]. This is not the case, as shown by the $\log_2 F_d(m)$ versus $\log_2 m$ plot in figure 10. In fact, the scaling behavior of figure 10 is not well defined, since those points do not form a nice straight line. Therefore, the Fourier truncation filtered data are not like a fBm-type random walk process. This is consistent with our earlier finding that the Fourier truncation filtered sunspot data still contain a significant cyclic trend.

doi:10.1088/1742-5468/2009/02/P02066

J. Stat. Mech. (2009) P02066

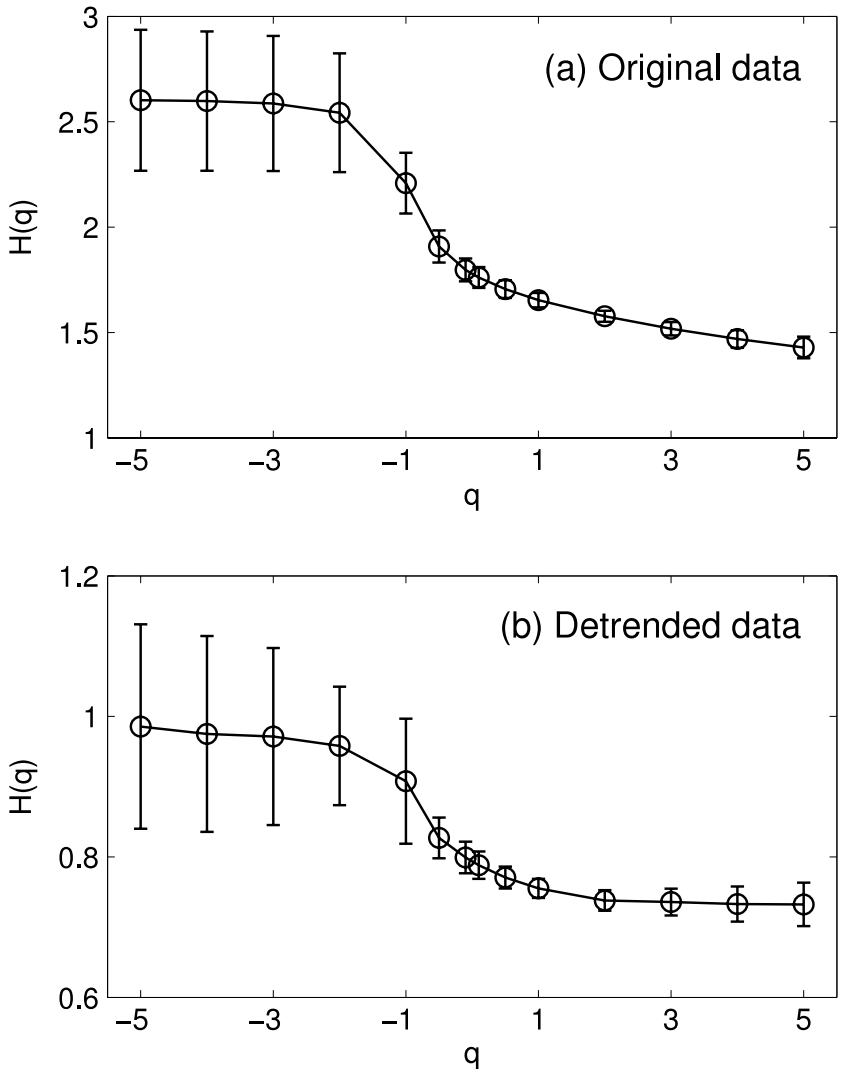

Figure 12. $H(q)$ spectrum for (a) the original and (b) adaptively filtered sunspot data.

3.4. MF-DFA of adaptively detrended sunspot data

We now analyze the adaptively obtained trend (the red curve of figure 1(a)) and the adaptively detrended data (equivalent to the difference between the original sunspot data and the red curve of figure 1(a)). The DFA results are shown in figure 11. We observe that the scaling exponent for the trend data is 1.92, again close to the value of 2 for a sinusoidal trend [19]. The scaling exponent for the detrended data is 0.74, close to that of figure 9(d). Again notice that the scaling region for the detrended data shown in figure 11 is only valid to m slightly smaller than 2^6 months, the same as for figure 9(d). Therefore, we can confidently conclude that $H \approx 0.74$ characterizes the correlation structure of the sunspot data with the 11-year cycle properly removed.

Next, we carry out MF-DFA of the original and adaptively detrended sunspot data (but not the trend data, since we clearly do not have a fractal signal). Their $H(q)$ spectra

J. Stat. Mech. (2009) P02066

are shown in figures 12(a) and (b), respectively. Since in both situations $H(q)$ varies with q significantly, we conclude that the original and the adaptively detrended sunspot data are multifractals. The fact that $H(q) > 1$ for the original sunspot data is of course due to the 11-year cycle of sunspots.

4. Concluding discussions

By designing an adaptive detrending algorithm to remove the 11-year cycle in sunspots and critically assessing the effectiveness of Fourier truncation in eliminating the 11-year cycle, we have found that Fourier truncation, being an operation that is physically not realizable, can only partially suppress the 11-year cycle in the sunspot data. The remaining trend can significantly interfere with the estimation of the fractal scaling exponents. When the 11-year cycle of the sunspot data is properly removed, a multifractal scaling with a correlation scaling exponent $H \approx 0.74$ emerges. Since $H > 0.5$, the detrended sunspot data have long-range correlations. The long-range correlations in sunspot variations signify that locally, an increase (or decrease) in sunspot number will be more likely followed by another increase (or decrease) in sunspot number. Therefore, if the 11-year cycle is viewed as a reference coordinate system, then a deviation of sunspot number from the cycle will be more likely followed by another deviation from the cycle on the same side. Properly accounting for this feature may help improve sunspot number prediction.

Acknowledgment

This work was partially supported by a NSF grant CMMI-0825311.

References

[1] R J Bray and Loughhead R E, 1979 *Sunspots* (New York: Dover)
[2] Zirin H, 1988 *Astrophysics of the Sun* (Cambridge: Cambridge University Press) chapter 10
[3] For illustrations of Maunder 'butterfly' diagram, we refer to http://sidc.oma.be/sunspot-index-graphics/sidc_graphics.php
[4] Temmer M, Veronig A and Hanslmeier A, 2002 *Astron. Astrophys.* **390** 707
[5] Bogart R S, 1982 *Sol. Phys.* **76** 155
[6] Veronig A, Messerotti M and Hanslmeier A, 2000 *Astron. Astrophys.* **357** 337
[7] Jevtic N, Schweitzer J S and Cellucci C J, 2001 *Astron. Astrophys.* **379** 611
[8] Abramenko V I, 2005 *Sol. Phys.* **228** 29–42
[9] Movahed M S, Jafari G R, Ghasemi F, Rahvar S and Tabar M R R, 2006 *J. Stat. Mech.* P02003
[10] McAteer R T J, Young C A, Ireland J and Gallagher P T, 2007 *Astrophys. J.* **662** 691
[11] Gao J B, Hu J, Tung W W, Cao Y H, Sarshar N and Roychowdhury V P, 2006 *Phys. Rev.* E **73** 016117
[12] Gao J B, Cao Y H, Tung W W and Hu J, 2007 *Multiscale Analysis of Complex Time Series—Integration of Chaos and Random Fractal Theory, and Beyond* (New York: Wiley–Interscience)
[13] Howe R, Christensen-Dalsgaard J, Hill F, Komm R W, Larsen R M, Schou J, Thompson M J and Toomre J, 2000 *Science* **287** 2456
[14] Wu Z H, Huang N E, Long S R and Peng C K, 2007 *Proc. Nat. Acad. Sci.* **104** 14889
[15] Chianca C V, Ticona A and Penna T J P, 2005 *Physica* A **357** 447
[16] Mandelbrot B B, 1982 *The Fractal Geometry of Nature* (San Francisco, CA: Freeman)
[17] Arneodo A, Bacry E and Muzy J F, 1995 *Physica* A **213** 232–75
[18] Peng C K, Buldyrev S V, Havlin S, Simons M, Stanley H E and Goldberger A L, 1994 *Phys. Rev.* E **49** 1685
[19] Hu K, Ivanov P Ch, Chen Z, Carpena P and Stanley H E, 2001 *Phys. Rev.* E **64** 011114
[20] Frisch U, 1995 *Turbulence—The Legacy of A N Kolmogorov* (Cambridge: Cambridge University Press)
[21] Gouyet J F, 1995 *Physics and Fractal Structures* (Berlin: Springer)
[22] Frederiksen R D, Dahm W J A and Dowling D R, 1997 *J. Fluid Mech.* **338** 127

J. Stat. Mech. (2009) P02066

[23] Mandelbrot B B, 1974 *J. Fluid Mech.* **62** 331
[24] Parisi G and Frisch U, *Fully developed turbulence*, 1985 *Turbulence and Predictability in Geophysical Fluid Dynamics and Climate Dynamics* ed M Ghil, R Benzi and G Parisi (Amsterdam: North-Holland) pp 71–84
[25] Gao J B and Rubin I, 2001 *Comput. Commun.* **24** 1400
[26] Gao J B and Rubin I, 2001 *Int. J. Commun. Syst.* **14** 783
[27] Tung W W, Moncrief M W and Gao J B, 2004 *J. Clim.* **17** 2736